Eur. Phys. J. D **39**, 399–405 (2006)
DOI: 10.1140/epjd/e2006-00112-5

THE EUROPEAN PHYSICAL JOURNAL D

Electron scattering by formic acid in the gas phase: comparing measured and computed angular distributions

F.A. Gianturco[1,a] and R.R. Lucchese[2]

[1] Department of Chemistry, University of Rome "La Sapienza", Piazzale A. Moro 5, 00185 Rome, Italy
[2] Department of Chemistry, Texas A&M University, College Station, Texas 77843-3255, USA

Received 24 March 2006 / Received in final form 19 April 2006
Published online 18 May 2006 –

Abstract. Elastic differential cross-sections are measured over a broad range of energy values and the results are compared with quantum calculations for the same process. The agreement between measured and computed data turns out to be fairly good and calculations further allow the separation of the cis and trans conformer behavior and to compare it with the angular distributions for scattering from the dimer at the same energies.

PACS. 34.80.Bm Elastic scattering of electrons by atoms and molecules – 34.80.-i Electron scattering

1 Introduction

The formic acid (HCOOH) molecule represents one of the simplest organic molecules which is expected to play a role in the interstellar formation of more complicated biomolecules [1]. Its dimer species, also a prototype for the carboxylic acid dimers, is one of the most stable neutral complexes and is known to form a ground state configuration of a cyclic, eight-membered ring that encompasses two strong hydrogen bonds [2,3]. The many studies on such systems have also led to the suggestion that both of them could be considered as key compounds in the formation of small biomolecules which can in turn provide the building blocks of larger biologically significant molecules in the early universe [4].

One further line of interest on this important molecule comes from the recent increase in the experiments that have established rather clearly how low-energy electrons are one of the main secondary products in biomaterials when irradiated by either energetic particles or by photons [5,6]. Such electrons are further capable of fragmenting the target biomolecules and become the chief initiators of the permanent damage effects, which are thus suggested to occur through the formation of highly reactive radicals and ions within the supporting medium [7].

The formic acid gaseous molecule has therefore been analyzed in terms of its behavior under impact of low-energy electrons [8] and the general interpretation of the observed resonances has been provided by our recent theoretical work [9]. The dimer species has also been observed experimentally in terms of fragmentation pattern under dissociative electron attachment (DEA) conditions [10] and has further been analyzed theoretically to provide a general attribution of the observed resonant patterns.

In the present work we carry out the analysis of experimental data which have recently become available [11] and discuss the computational and theoretical behavior of the electron angular distributions under elastic scattering conditions for the gas-phase monomer species. The next section will therefore briefly outline the computational and theoretical treatment for the elastic (rotationally summed) differential cross-sections (DCS). Section 3 will then compare the measured data with the calculations and Section 4 will present our conclusions.

2 The computational machinery: an outline

2.1 The scattering equations

Within the Born-Oppenheimer (BO) approximation the total wave function of a continuum electron that scatters from an N-electron molecular target is an antisymmeterized product of one-electron orbitals which parametrically depend on the nuclear coordinates. Our present treatment of the scattering process is limited to an analysis of the elastic channels and no excitations will be considered for either the bound electrons or the bound nuclei. In fact, we will describe the scattering within the fixed-nuclei (FN) approximation [12], which neglects any dynamics involving the nuclear motion, whereas the bound electrons will be taken to be in the ground electronic state of the target at its optimized nuclear geometry. The initial description of that state will be given as a single-determinant of near-Hartree-Fock molecular orbitals (MOs) describing

[a] e-mail: fa.gianturco@caspur.it

the N-bound electrons. To obtain our scattering equations we then expand both the bound MOs and the continuum electron in a single-center expansion (SCE) around the center of mass of the target by employing symmetry-adapted angular functions for each of the irreducible representations (IRs) that belong to the molecular point-group at the chosen geometry of its nuclei. Any arbitrary three-dimensional single-electron function is thus represented on a spherical-polar coordinate grid centered in the body-fixed (BF) molecular frame of reference:

$$F^{p\mu}(r,\hat{\mathbf{r}}|\mathbf{R}) = \sum_{l,h} r^{-1} f_{lh}^{p\mu}(r|\mathbf{R}) X_{lh}^{p\mu}(\hat{\mathbf{r}}). \quad (1)$$

The indices refer to the μth element of the pth IR of the point group of the molecule at the nuclear geometry $\mathbf{R}$. The angular functions $X_{lh}^{p\mu}(\hat{\mathbf{r}})$ are symmetry-adapted functions given by the proper combination of spherical harmonics $Y_{lm}(\hat{\mathbf{r}})$:

$$X_{lh}^{p\mu}(\hat{\mathbf{r}}) = \sum_{m} b_{lmh}^{p\mu} Y_{lm}(\hat{\mathbf{r}}) \; . \quad (2)$$

The coefficients $b_{lmh}^{p\mu}$ are discussed in the literature [12] and we will not discuss them here any further.

The coupled partial integro-differential scattering equations are

$$\left[\frac{d^2}{dr^2} - \frac{l(l+1)}{r^2} + 2(E-\epsilon_\alpha)\right] f_{lh}^{p\mu\alpha}(r|\mathbf{R}) = 2 \sum_{l'h'p'\mu'\beta} \int dr' V_{lh,l'h'}^{p\mu\alpha,p'\mu'\beta}(r,r'|\mathbf{R}) f_{l'h'}^{p'\mu'\beta}(r'|\mathbf{R}), \quad (3)$$

where E is the collision energy and ϵ_α the electronic eigenvalue for the target ground state so that $(E-\epsilon_\alpha) = k^2/2$, where k is the asymptotic momentum of the scattered electron. The (p,μ) indices, in equation (3), now label the specific μth component of the pth IR that characterizes the continuum that belongs to the αth electronic target state (initial state) coupled with the excited states labelled by β with the corresponding continuum symmetry labelled by (p',μ'). Equation (3) contains the kernel of the integral operator V, a sum of diagonal and non-diagonal terms that in principle fully describe the electron-molecule interaction during the collision. If one now further truncates the sum on the right-hand side of equation (3) to a single state only, one obtains the exact-static-exchange (ESE) representation of the electron-molecule interaction for the ground state at the geometry $\mathbf{R}$.

When one restricts the summation in equation (3) to a single state the effects of static and dynamic electron-electron correlation are neglected. The static correlation asymptotically produces the long-range multipolar polarization of the target and is of prime importance for low-energy electron scattering processes. We therefore include here a modelling of the dynamical short-range correlation through the addition of a local energy-independent potential $V_{\rm corr}$ which we have discussed many times before [12]. The short-range potential $V_{\rm corr}$ is then obtained from an average dynamical correlation energy of a single electron within the formalism of the Kohn and Sham variational scheme (see also [13] for details). The functional derivative of such a quantity with respect to the N-electron density provides a density functional description of the required short-range correlation term, this being an analytic function of the target ground-state electron density. When studying the full scattering problem, we usually correct the large r behavior of $V_{\rm corr}$ so that it agrees with the known static polarizability of the target molecule [9].

2.2 The angular distributions

The main quantities obtained from the asymptotic behavior of the $f_{lh}^{p\mu}(r|\mathbf{R})$ of equation (3) are the matrix elements of the T-matrix, $T_{ll'}^{p\mu}\left(k^2|\mathbf{R}\right)$ which are produced in the Body-Fixed (BF) frame of reference and are them transformed to the Space-Fixed (SF) frame via a well-known unitary transformation [13].

When one is dealing with polar molecules like HCOOH, however, the leading term of the long-range interactions, in the BF frame, is given by $\sim(D(\mathbf{R})/r^2)P_1(\cos\theta)$ which is a very long-range interaction causing the FN approximation to fail [14]. The corresponding divergence of the angular distributions in the forward direction comes basically from the fact that the above T-matrix elements go to zero very slowly so that the sum over (l,l') needed to obtain the DCS does not converge and the integral cross-section diverges logarithmically [15]

$$\sigma(k^2) \propto \frac{4\pi}{3k^2} D^2 \sum_{l=0}^{\infty} \left(\frac{1}{l} + \frac{1}{l+1}\right). \quad (4)$$

In qualitative terms one could say that the cross-sections could be treated as being the sum of two distinct parts, one which includes the contributions of the smaller (l,l') values of the T-matrix elements, while the second one includes the further contributions from the larger (l,l') values of the additional T-matrix elements (with Λ now collectively indicating the $|p\mu\rangle$ indices)

$$\sigma = \sum_{\Lambda} \sum_{l,l'=0}^{l''} C_{l,l',\Lambda} |T_{l,l'}^{\Lambda}|^2 + \sum_{\Lambda} \sum_{l,l'>l''}^{\infty} C_{l,l',\Lambda} |T_{l,l'}^{\Lambda}|^2. \quad (5)$$

The $T_{l,l'}^{\Lambda}$ matrix elements are in turn related to the $f_{l,l'}^{p\mu}$ radial functions of equation (3) and these functions, for the smaller (l,l') values originate from the action of both long-range part of the potential and of its short-range-part. However, the phase accumulation that comes from the long-range part of the potential is fairly small with respect to the phase accumulation that comes from the short-range part of the interaction, due to the stronger coupling caused by the latter. Hence in practice the phase accumulation of the smaller (l,l') values of $f_{l,l'}^{\Lambda}(r)$, will mainly be determined by the short-range part of the potential acting on the incoming electron.

On the other hand, the contributions to the cross-section which come from large (l, l') values will be determined by the coefficients of the larger partial waves. The particles with these trajectories sample a much larger centrifugal potential which can keep them away from the inner region. In such cases, their phase accumulation effects will be mainly caused by the long-range part of the potential. For this reason, one can identify the contributions from the larger partial waves to the cross-section with the contribution from the same partial waves of the simpler case in which the potential is only given by the dipole potential for any r, i.e. for the problem of a fixed dipole scatterer. This approximation, on the other hand is known to give infinite cross-section [14]. It therefore follows that the contributions from the larger partial waves in the case of polar molecules are also diverging. However, if the rotational term is not disregarded in the chosen Hamiltonian the solutions become again well-behaved [16]. What one can therefore do in practice is to replace the contributions to the T-matrix for the larger (l, l'') with the same elements calculated for the dipole rotor as the only scattering potential.

It is worth reminding ourselves that the breakdown of the FN approximation for polar molecules is a consequence of disregarding the rotational part of the Hamiltonian of the problem, hence it is an artifact introduced by the physical approximation implied by the above reduction of the total, exact Hamiltonian. Such artifacts would still be present if we were to treat the collision in either the BF or SF frames of reference since they are directly related to the FN simplification.

Thus, the DCS for the scattering into a polar angle θ in the SF frame of reference can be expressed as a Legendre expansion [13]

$$\frac{d\sigma}{d\Omega}(vj \to v'j') = \sum_{\lambda=0}^{\infty} A_\lambda(vj \to v'j') P_\lambda(\cos\theta). \quad (6)$$

The coefficients $A_\lambda(vj \to v'j')$ now depend explicitly on the product of the elements of the transition matrix T with some algebraic factor in a way which is reported in detail in earlier work [16]. The $A_\lambda(vj \to v'j')$ involve an infinite sum over the angular momenta l and l' of the T matrix elements. The integral cross-section (ICS), involves only the A_0 coefficient while the momentum transfer cross-section involves the A_0 and A_1 coefficients [16]

$$\sigma = 4\pi A_0 \quad (7)$$

$$\sigma^M = 4\pi \left(A_0 - \frac{1}{3} A_1 \right). \quad (8)$$

If we would use the T matrix elements as obtained by solving the FN Hamiltonian, we know that the DCS would diverge for $\theta = 0$ and would take oscillating values for $\theta \neq 0$ because the contributions of the long-range part of the potential (given by the same expression as that for the fixed dipole) cannot be expanded in a Legendre series [14]. If we were to use the full Hamiltonian, on the other hand,in order to describe the small-angle scattering we would need

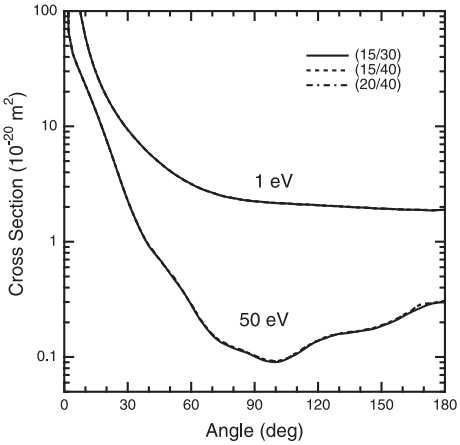

Fig. 1. Computed DCS at two different energies and for different descriptions of the low-l contributions to the cross-sections. The expansions for each calculation are indicated as ($l_{\max}$ SEP/$l_{\max}$ SMEP).

many A_λ coefficients in equation (6) because that expression is slowly convergent for polar molecules, and consequently many T matrix elements are needed. This is due to the fact that, for polar molecules, the T matrix elements with large (l, l') give the main contributions to the DCS. For $\theta = 0$ the solution of the dipole rotor scatterer (which is the same as the solutions which employ a real potential for small angle scattering) behaves as $1/(1-(1+\varepsilon)\cos\theta)$ and therefore the expansion of this term is slowly convergent [18]. In practice, one has the difficulty that to describe the DCS for small-angle scattering one must employ an increasingly larger number of partial waves as the scattering angle decreases. Although it should be clear by now where the FN approximation is failing (i.e. in the evaluation of the T matrix elements for large l, as the sums over these elements cause the divergence) one would still like to be able to extract as much information as possible from a calculation which employs such a simple form of the Hamiltonian. It could therefore become expedient to replace the high l contributions with those coming from the dipole rotor scatterer as the latter does not suffer from the divergence. However, this could not be done simply by replacing the FN T matrix elements with the correct ones in equation (6), because this procedure may help to solve the problem of the forward divergence but would not help to solve the basic difficulty of the slow convergence as one now would still need a very large number of T matrix elements, One possible alternative is to use instead a closure formula

$$\frac{d\sigma}{d\Omega}(vj' \to v'j') = \frac{d\sigma^{\mathrm{FBA}}}{d\Omega}(vj \to v'j') + \Delta\frac{d\sigma}{d\Omega}(vj \to v'j') \quad (9)$$

where

$$\Delta\frac{d\sigma}{d\Omega}(vj' \to v'j') = \frac{1}{4k_{vj}} \sum_{\lambda=0}^{\infty} [A_\lambda(vj' \to v'j') - A_\lambda^{\mathrm{FBA}}(vj' \to v'j')] P_\lambda(\cos\theta). \quad (10)$$

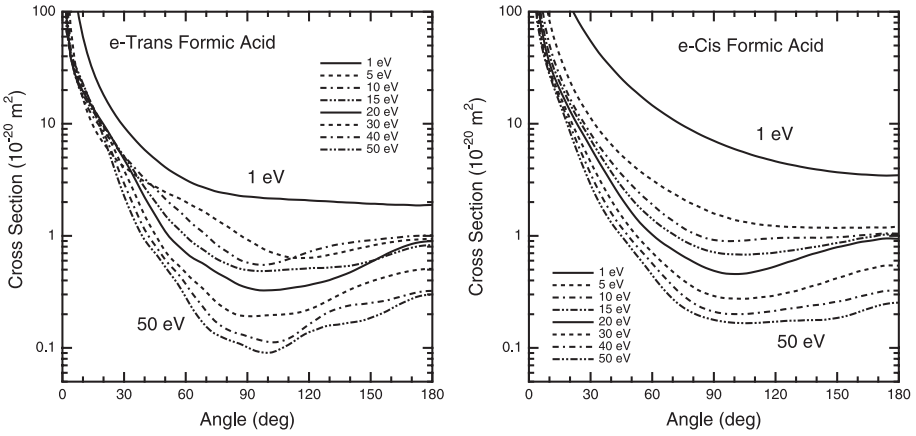

Fig. 2. Computed angular distributions for the cis (left panel) and trans (right panel) conformers as a function of the collision energy.

This formula is written [19] in its generalized form for rovibrational excitations but obviously can also be applied to elastic processes. The first term in equation (9) is the first Born approximation (FBA) for the differential cross-section for which simple closed-form expressions are available [15]. On the other hand, the second term represents its partial wave expression which also includes the formulation of the T-matrix elements in the FBA form, already available in the literature [15]. The sum over λ converges much more rapidly and terminates at $\lambda_{\max}$ while the contributions to any A_λ for $l(l') \geq l_{\rm FBA} + \lambda$ cancel each other identically. Therefore, the elements of T from exact calculations are now required for a limited range of values only. In a sense, one can say that a separation of the angular ranges contributing to the cross-sections has now been achieved. For equation (9) to be an equality it is further necessary that the first term of this equation and the second one from equation (10) be identical. However, to obtain a difference $(A_\lambda - A_\lambda^{\rm FBA})$ that becomes zero for high λ one must use the T-matrix elements from the fixed dipole scatterer. Thus, we would eliminate the problem of oscillations for angles different from 0°, because both A_λ and $A_\lambda^{\rm FBA}$ represent oscillating quantities when increasing the dimensions of the T matrix, as previously explained: i.e. the high λ's contain high l's T-matrix elements which feel mainly the dipole potential, hence they must be equal to those elements from the fixed dipole scatterer which cannot be expanded into Legendre polynomials.

3 Computing the differential cross-sections

The target wave function and geometry were those already described in our earlier calculations of reference [9]. The partial wave expansion was tested in the trans geometry of HCOOH. The range of the low l values was extended from 15 to 20 using exact static-exchange-polarization (SEP) calculations and was further extended to $l = 40$ using a model, semiclassical exchange already described in our earlier work (SMEP) [13]. The FBA values were then used in equations (9) and (10) to provide a further test of the convergence. An example of this analysis is shown by Figure 1, where two different energy values are examined (1.0 eV and 50.0 eV) and the different expansions

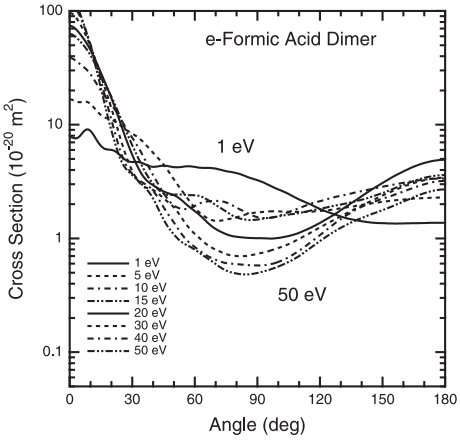

Fig. 3. Computed elastic (rotationally summed) angular distributions for electron scattering off FAD molecules at different collision energies.

are compared: one clearly sees that only small differences exist for the lower-l expansions, while the final results are fully converged at all angles.

A comparison of the behavior of the cis and trans-configurations for the formic acid (FA) is shown over a broad range of energies by the two panels reported in Figure 2. We show there the full exchange calculations ($l_{\max} = 30$) for different collision energies from 1.0 eV up to 50 eV. One clearly sees the very marked similarities (as expected) of the two systems, with the trans configuration showing deeper DCS minima around $\theta \sim 90°$ than the cis configuration. Both sets of data, however, present strong forward scattering features and a very marked increase of cross-section "dips" around 90° as the collision energy increases. The dominance of the dipole scattering is, however, evident from all calculations.

A rather different behavior of the scattered electron distributions is shown, however, by the case of the formic acid dimer (FAD), which we had studied earlier in terms of resonant structures [17] and for which we have now computed the DCS using the same target structure of [17] and carrying out the same convergence study already outlined for the FA target before.

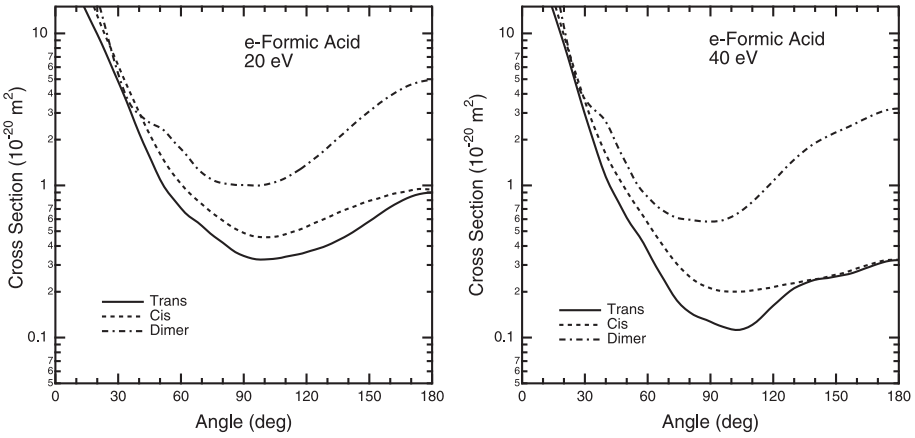

Fig. 4. Computed angular distributions, at 20 eV (left panel) and 40 eV (right panel) for the two conformers of the FA molecule and for the FAD molecular target.

The results reported by Figure 3, over the same range of energies already examined for the FA molecule, show a different behavior than before. We see, in fact, that the low-energy DCS present no marked intensity dips around 90°, while a modest intensity reduction begins to appear from about 20 eV and above. The different target symmetry and the presence of a stronger selection rule for the contributing angular momenta [17] indicate that the interference effects are weaker in the dimer case with respect to the monomer, where the lower symmetry (A') allows for stronger interference effects in the computed DCSs.

That this is indeed the possible explanation could be gleaned from a comparison carried out at two different collision energies and reported by the two panels of Figure 4. We show there the FA angular distributions for the two conformers and also the one for the FAD complex: at both energies one sees that the trans configuration shows the strongest intensity decreases as θ increases, while the FAD target presents at both energies very marked backward scattering features and rather modest intensity reduction as θ approaches $\pi/2$.

In conclusion, our calculations indicate that angular distribution should be able to show differences between the two FA conformers and also suggest that the presence of FAD molecules would show up in the DCS behavior.

In the following section we therefore compare our results with the experiments to find out both how well we are reproducing them and whether or not the measurements bear us out in showing possible differences between the behavior of the different conformers.

4 Comparing experiments and calculations

We have decided to compare both our calculations for the two conformers of FA with the experimental findings in order to see if one could detect differences in the experiments which would indicate the dominant species.

The four panels of Figure 5 therefore report the experimental data at four different energies [11] and the results of our calculations for both the cis and trans conformers. One clearly sees there that all our computed data follow quite closely the experiments, especially in the forward direction, and agree with them in showing the presence of an intensity "dip" around 90°. In fact, the calculations show that feature to be more marked for the trans isomer than for the cis isomer, while the experiments, from 5 eV up to 15 eV, indicate a less marked minimum and appear to be better described by the cis configuration calculations.

The comparison at higher collision energies is shown by Figure 6, where we report in its four panels the data at four different energies, from 20 to 50 eV. The data at higher energies show the experiments [11] to have a stronger increase in the backward direction than that surmised by our calculations. The computed data for the cis conformer are again following measurements more closely in the intermediate angular region. In any event, these higher energy data indicate a much stronger backward scattering component than that provided by our calculations. However, considering the importance of correlation effects in this region of interaction, we think that our model treatment of correlation-polarization forces in the intermediate and short-range of distance is probably the main cause for the observed discrepancies as the collision energy increases.

5 Present conclusions

We have carried out calculations for the angular distributions of scattered electrons off the gas-phase FA molecule over a broad range of collision energies and corresponding to the elastic (rotationally summed) channels at the considered energies.

The calculations turn out to be in reasonable agreement with experiments [11], producing the strong forward peaking observed at all energies, as expected for a polar molecular target, and reproducing the marked dip in distribution intensities near $\theta = \pi/2$. The experiments in the higher energy range ($E > 15$ eV) [11] also show a marked increase of intensity in the backward direction, a feature which is only in part described by our calculations. The latter, however, do confirm the presence of sizeable DCS values as θ increases towards π.

Our calculations are able to compare the angular distributions produced by the two possible cis and trans

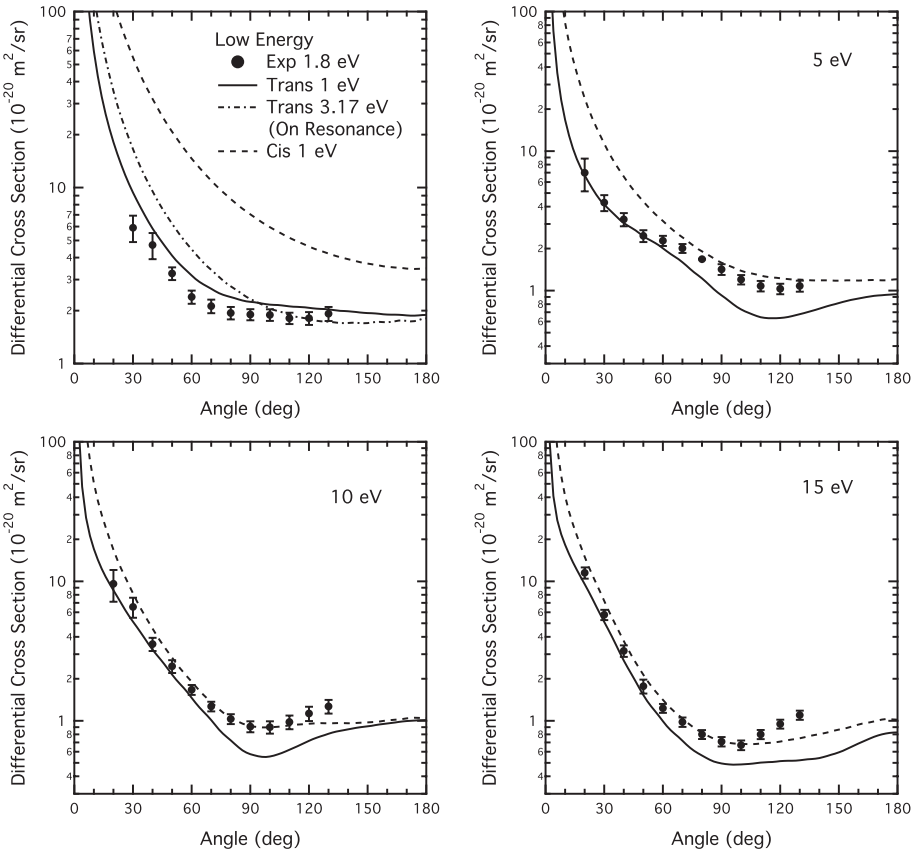

Fig. 5. Computed and measured [11] angular distributions for the elastic DCS (rotationally summed). The calculations refer to the trans isomer (solid line) and to the cis isomer (dashed line).

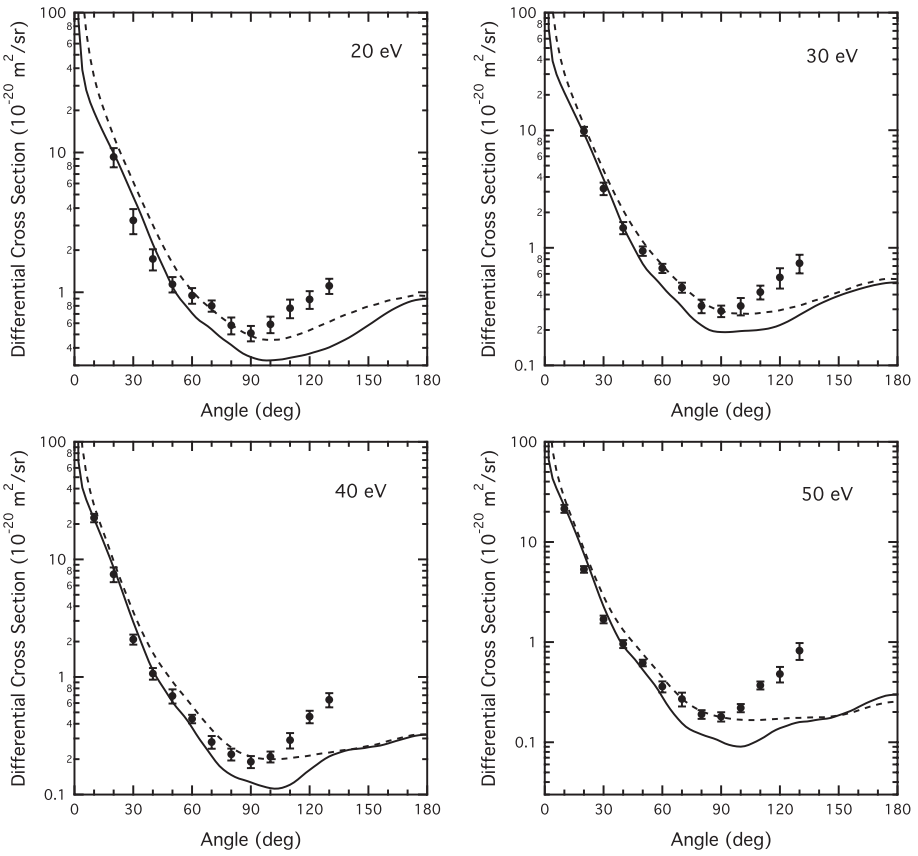

Fig. 6. Computed and measured (from Ref. [11]) elastic differential cross-sections (rotationally summed) for the cis (dashed) and trans (solid lines) conformers of the FA molecule.

configurations of the FA molecule in the gas phase. Our calculations for the isolated molecule [9] indicate the trans structure to be more stable by about 0.169 eV, although no zero point energy correction was applied to estimate that value. The corresponding scattering results show that, over the whole range of considered energies, the cis target produces a less marked intensity dip around $\theta = \pi/2$ in comparison with the trans configuration. The corresponding experiments do seem to be more closely reproduced by the cis data although we think that the present calculations are not accurate enough to be able to really distinguish between the two contributions on the basis of the overall agreement with experiments.

Another test calculation that we were able to carry out involved the behavior of the DCS, over the same range of collision energies, for the gas-phase dimer complex, the FAD molecule which we had already studied, experimentally and theoretically, in our previous work [17] in terms of resonant features.

The present numerical analysis clearly shows that one should expect a different angular behavior for the FAD target species: the forward scattering peak is certainly present also in this case, but the marked decrease around $\theta \sim \pi/2$ is much less visible and does not come up in the distributions at the lower-end (1 eV to 5 eV) of the examined energy scale. In other words, the calculations suggest that the experiments which were to be able to identify unequivocally scattering from FAD species, should also produce data which differ considerably from the corresponding monomer distributions and should therefore be amenable to experimental detection.

The financial support of the University of Rome I Research Committee, of the European Network EPIC (HPRN-CT-2002-00286) and of the Welch Foundation (Grant No. A-1020) are gratefully acknowledged. we are also grateful to Professor Stephen Buckmann for many helpful discussions and for providing us with the experimental data prior to publication.

References

1. E.g. see: W.M. Irvine, P. Friberg, N. Kaifu, Y. Kitamura, K. Kawaguchi, Astrophys. J. **342**, 871 (1989)
2. F. Madeja, M. Havenith, J. Chem. Phys. **117**, 7162 (2002)
3. J. Chocholousova, J. Vacek, P. Hobza, Phys. Chem. Chem. Phys. **4**, 2119 (2002)
4. F. Ban, J.W. Gould, R.J. Boyd, J. Phys. Chem. A **104**, 10159 (2000)
5. J.A. La Verne, S.M. Pinblot, Rad. Res. **141**, 208 (1995)
6. L. Sanche, Mass Spectrom. **21**, 349 (2002)
7. B. Boudaiffa, P. Calutier, D. Hunting, M.A. Huels, L. Sanche, Rad. Res. **157**, 227 (2002)
8. A. Pelc, W. Sailer, P. Scheier, M. Probst, N.J. Manson, E. Illenberger, T.D. Maerk, Chem. Phys. Lett. **361**, 277 (2002)
9. F.A. Gianturco, R.R. Lucchese, New J. Phys. **6**, 66 (2004)
10. I. Martin, T. Skalicky, J. Langer, H. Abdoul-Carime, G. Karwasz, E. Illenberger, M. Stano, S. Matejcik, Phys. Chem. Chem. Phys. **7**, 2212 (2005)
11. V. Vizcaino, M. Jelisaucic, J.P. Sullivan, S.J. Buckmann (unpublished results)
12. E.g. see: F.A. Gianturco, A. Jain, Phys. Rep. **143**, 347 (1986)
13. F.A. Gianturco, R.R. Lucchese, Int. Rev. Phys. Chem. **15**, 429 (1996)
14. For details see: N.F. Lane, Rev. Mod. Phys. **52**, 29 (1980)
15. D.W. Norcross, L.A. Collins, Adv. At. Mol. Phys. **18**, 341 (1982)
16. N. Chandra, Phys. Rev. A **12**, 2342 (1975)
17. F.A. Gianturco, R.R. Lucchese, J. Langer, I. Martin, M. Stano, G. Karwasz, E. Illenberger, Eur. Phys. J. D **35**, 417 (2005)
18. For details see: F.A. Gianturco, P. Paioletti, in: *Novel Aspects of Electron-Molecule Collisions*, edited by K.H. Becker (World Scientific, Singapore, 1998), p. 57
19. W.R. Garrett, Phys. Rev. A **4**, 2229 (1971)